iScience

Article

$CsPbBr_3$ perovskite nanoplatelets capped with inorganic ligands for stable deep blue emission

Graphical abstract

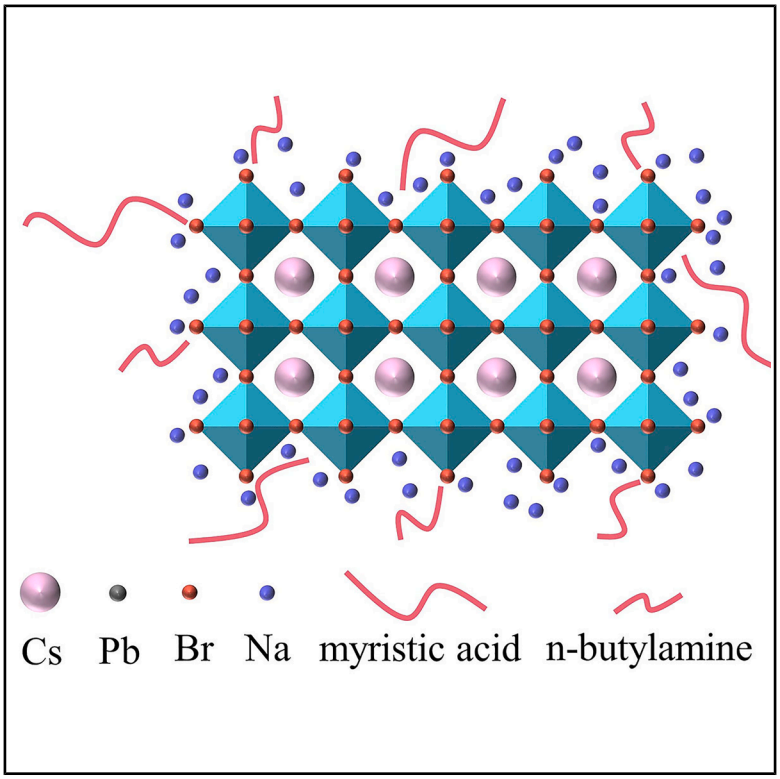

Highlights

- $CsPbBr_3$ nanoplatelets have been synthesized successfully by LARP method
- The mechanism of inorganic ligand has been explained
- The as-synthesized samples were used as blue source for the LED device

Authors

Anqi Zhang, Zhiqi Yao, Chun Sun, ..., Danbi Kim, Xinyu Shen, Sung Heum Park

Correspondence

shenxinyu93@gmail.com (X.S.), spark@pknu.ac.kr (S.H.P.)

In brief

Chemistry; Inorganic chemistry; Materials science; Nanomaterials

Zhang et al., 2025, iScience *28*, 114078
December 19, 2025
https://doi.org/10.1016/j.isci.2025.114078

CellPress

iScience

CellPress
OPEN ACCESS

Article

$CsPbBr_3$ perovskite nanoplatelets capped with inorganic ligands for stable deep blue emission

Anqi Zhang,[1] Zhiqi Yao,[2] Chun Sun,[3] Bo Ram Lee,[4] Jiaxin Song,[4] Zhengtong Wang,[3] Ying Li,[2] Fengwu Liu,[2] Eunhye Yang,[2] Danbi Kim,[2] Xinyu Shen,[5,*] and Sung Heum Park[2,6,*]

[1]Key Laboratory of Low-dimensional Structural Physics and Application, Education Department of Guangxi Zhuang Autonomous Region, College of Physics and Electronic Information Engineering, Guilin University of Technology, Guilin 541004, P.R. China
[2]Department of Physics, Pukyong National University, Busan 48513, Republic of Korea
[3]State Key Laboratory of Reliability and Intelligence of Electrical Equipment and Tianjin Key Laboratory of Electronic Materialsand Devices, School of Electronics and Information Engineering, Hebei University of Technology, 5340 Xiping Road, Tianjin 300401, P.R. China
[4]School of Advanced Materials Science and Engineering, Sungkyunkwan University, Suwon 16419, Republic of Korea
[5]Clarendon Laboratory, Department of Physics, University of Oxford, Oxford OX1 3PU, UK
[6]Lead contact
*Correspondence: shenxinyu93@gmail.com (X.S.), spark@pknu.ac.kr (S.H.P.)
https://doi.org/10.1016/j.isci.2025.114078

SUMMARY

All-inorganic halide perovskite materials have attracted significant interest for display applications because of their narrow bandwidths and high photoluminescence quantum yields. However, the development of blue-light-emitting perovskite materials has been slower than that of green- and red-light-emitting perovskites. In this study, we successfully produced single-halide $CsPbBr_3$ nanoplatelets with a quantum confinement effect using ligand-assisted reprecipitation techniques. NaBr, an inorganic ligand with strong binding affinity (adsorption energy, −2.13 eV) and low steric hindrance, was used to prevent the continued growth of nanoplatelets. A series of experimental results demonstrate that $CsPbBr_3$ nanoplatelets with a dense Na^+ shell on the surface exhibit stable deep blue emission. UV chip-based light-emitting devices activated by these nanoplatelets demonstrated remarkable spectral stability as the current injection increased. Moreover, the synthesis process is conducted under simple conditions at room temperature, demonstrating potential for batch production.

INTRODUCTION

In recent years, all-inorganic cesium lead halide ($CsPbX_3$, X = I, Br, Cl) perovskite nanocrystals (NCs) have been extensively explored owing to their cost-effective synthesis, tunable bandgaps, and high color purity.[1,2] Although the $CsPbX_3$ NCs have been considered as ''defect-tolerant'' nanomaterials compared with traditional metal chalcogenide NCs,[3] the photoluminescence (PL) quantum yields (PLQYs) of blue light-emitting $CsPb(Cl/Br)_3$ NCs still lag far away from the near unity of the green light- and red light-emitting perovskite NCs due to the mid-gap traps caused by chlorine vacancies.[4,5] The $CsPb(Cl/Br)_3$ NCs still suffer from seriously irreversible phase segregation into separate chlorine- and bromide-rich domains, even after the implementation of enhanced strategies such as post-treatment and divalent or trivalent cation doping,[6,7] due to halide ion migration with the impact of light or an electronic field, resulting in emission instability and limited applications.[8,9] Consequently, the development of blue perovskite light-emitting device (LED) has not progressed at the same pace as that of green and red LEDs, particularly regarding color purity and stability.[10,11] Although significant advancements have been achieved in the development of sky blue polymer LEDs within the wavelength range of 480–495 nm, these devices still do not meet the specifications for the blue primary color requirement (467 nm) as defined in the Rec. 2020 color space. Therefore, the research and development of deep blue perovskite with wavelength shorter than 470 nm holds significant importance.[12,13] One of the recent strategies for enhancing device properties involves component engineering aimed at optimizing the emission characteristics of blue perovskite materials.[14,15]

In this circumstance, the two-dimensional (2D) single halide $CsPbBr_3$ nanoplatelets (NPLs) with quantum confinement effect become an attractive candidate that protects the blue-emitting perovskite from halide segregation issues.[16] The emission peak of $CsPbBr_3$ NPLs can be tuned from 497 to 432 nm by adjusting the Cs/Pb ratio in the precursor synthesized through a reprecipitation method at room temperature.[17] The ligand-assisted reprecipitation (LARP) method has been extensively employed for the synthesis of perovskite NCs.[18–20] As we all know, abundant surface defects will be left with the desorption of ligands during the synthesis and purification processes, which

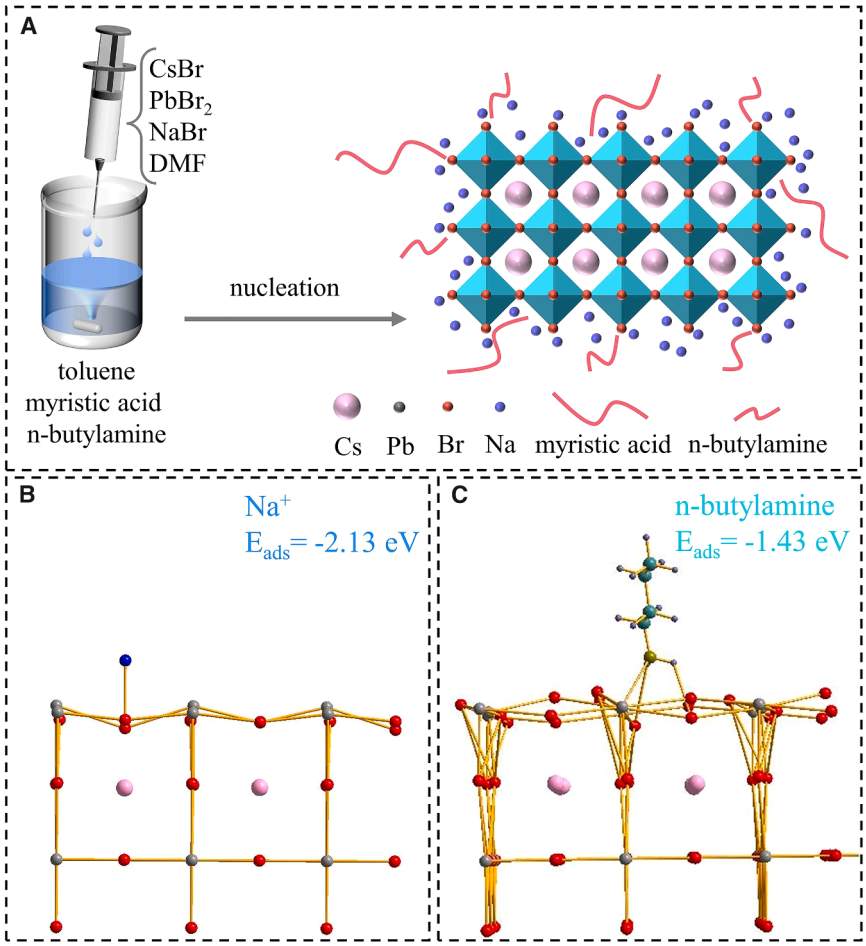

Figure 1. Synthesis of $CsPbBr_3$ nanoplatelets and its first-principles calculations

(A) Schematic diagram illustrating the synthesis of $CsPbBr_3$ nanoplatelets.

(B and C) (B) Theoretical model for protonated n-butylamine and (C) Na^+ adsorbed on the surface of $CsPbBr_3$ NPLs. The Br atoms are the preferred adsorption sites for Na^+ and protonated n-butylamine.

do harm to the PLQY of perovskite materials, especially for NPLs with 2D structures.[21–23] Surface engineering to passivate defects can be realized by the introduction of organic capping molecules or inorganic ligands.[24,25] For example, $CsPbBr_3$ NPLs are post-treated with oleylammonium fluoride salt, potassium bromide, zinc bromide, 2-butynoic acid, etc. By forming Pb–F bonds, K–Br bonds, and Zn–Br bonds on the surface, the formation of Br vacancies is inhibited.[26–29] It is noteworthy that the cases mentioned primarily use long-chain ligands for synthesizing NPLs. Replacing these with shorter-chain ligands during synthesis can significantly improve the carrier transport efficiency of NPLs.[30] However, short chains fail to offer adequate stabilization, leading to inadequate colloidal stability and low PLQYs.[31,32] Herein, we synthesized blue-emitting $CsPbBr_3$ NPLs with inorganic ligands (NaBr) and short organic ligands (myristic acid and n-butylamine) capped using LARP. Compared with the hot injection method, which requires high temperature and an inert gas atmosphere,[33] the LARP method can be performed at room temperature under ambient air, significantly reducing production costs and complexity. Subsequently, density functional calculations revealed that the inorganic ligand (NaBr) has a greater binding affinity to the NPL surface than the organic ligand. Inorganic ligands effectively bind to the NPL surface, controlling the NPL growth kinetics; meanwhile, the surface defects of the NPLs are passivated in the Br-rich environment. The $CsPbBr_3$ NPLs capped with an inorganic ligand displayed stable deep blue PL emission at 460 nm.

RESULTS AND DISCUSSION

Synthesis and characterization of $CsPbBr_3$ NPLs

$CsPbBr_3$ NPLs were synthesized using a modified LARP method, as shown in Figure 1. Appropriate amounts of CsBr, $PbBr_2$, and the inorganic ligand NaBr were dissolved in N,N-dimethylformamide (DMF) to form a clear transparent precursor solution.[34] The precursor solution was then injected swiftly into toluene containing the short organic ligands, myristic acid and n-butylamine, with vigorous stirring at room temperature. After completion of the reaction, processes such as centrifugal purification are carried out. The specific details are presented in the experimental section. To investigate the interaction of NaBr with the $CsPbBr_3$ NPLs, we calculated the adsorption energy of Na^+ and $C_4H_{11}N$ on $CsPbBr_3$ NPL surface (Figure S1) using density functional theory (DFT) calculations (Figures 1B and 1C). The Na^+-capped $CsPbBr_3$ NPL surface shows a larger adsorption energy (E_{ads} −2.13 eV) than that of the protonated n-butylamine-capped surface (−1.43 eV), indicating a stronger binding affinity between Na^+ ions and the perovskite surface, which is beneficial to stabilize the NPL surface.[35] Additionally, both Cs and Br vacancy defects can be passivated in the NaBr-rich environment, giving rise to a boosted radiative recombination of the $CsPbBr_3$ NPLs.

Transmission microscopy (TEM) and high-resolution TEM (HRTEM) images of the NaBr-capped $CsPbBr_3$ NPLs are shown in Figure 2A and the inset, respectively. The corresponding HRTEM image shows high crystallinity with a lattice distance of 0.2984 nm, corresponding to the (200) crystal planes of $CsPbBr_3$. As shown in Figure S2, the NaBr-capped NPLs have a thickness of 3.55 nm. TEM of $CsPbBr_3$ samples without NaBr coating revealed a nanocube morphology with increased thickness (Figure S3). The crystal structure of the NPLs was verified using X-ray diffraction (XRD) (Figure 2B). The diffraction peaks at 15.1° and 30.4° of both $CsPbBr_3$ NPLs with and without

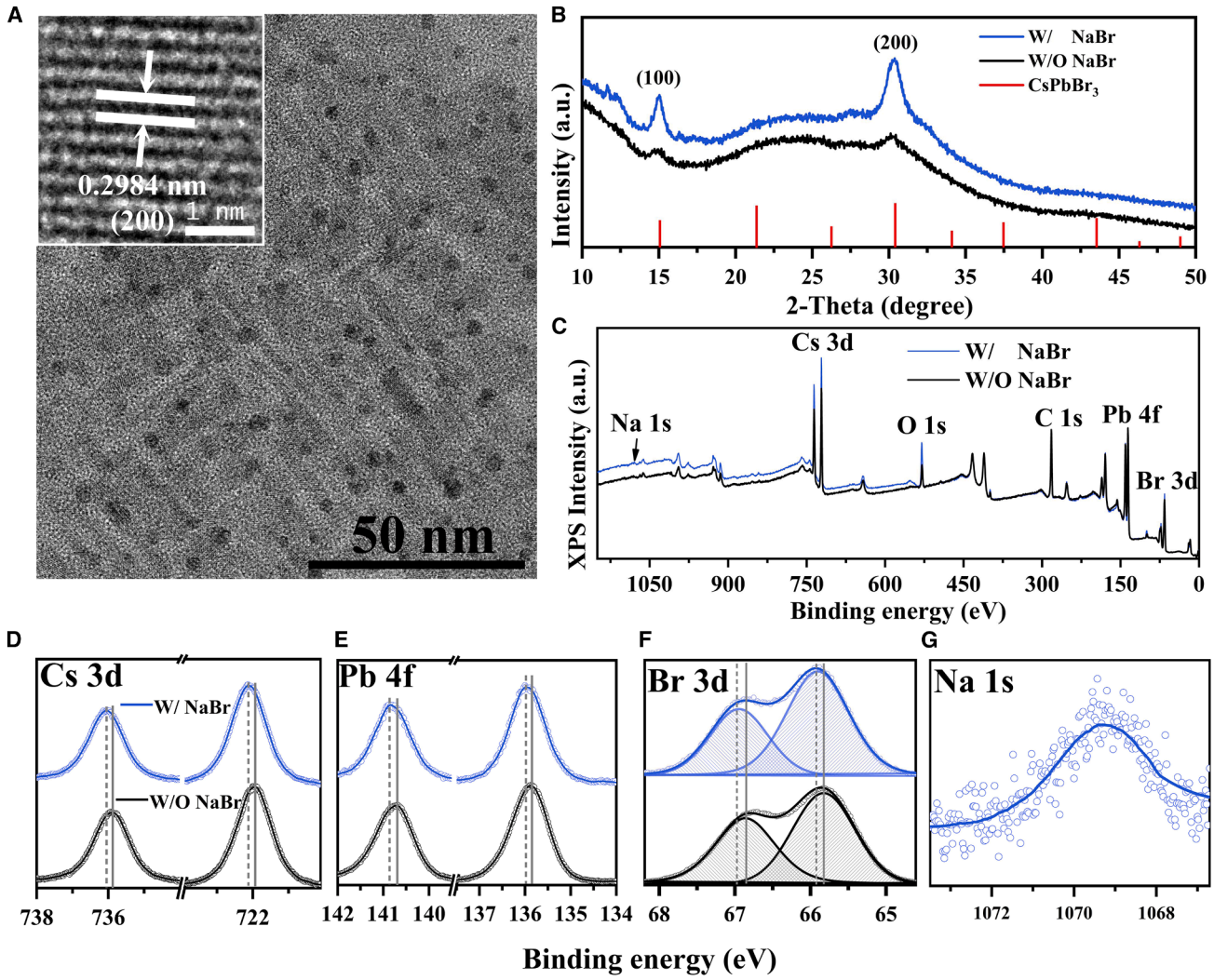

Figure 2. TEM, XRD, and XPS characterization

(A) TEM images of $CsPbBr_3$ NPLs (the inset shows the HRTEM images). Scale bar, 50 nm.

(B) XRD patterns of the samples without and with NaBr.

(C–G) (C) XPS spectra of $CsPbBr_3$ NPLs; (D–F) XPS spectra of the samples for Cs 3d, Pb 4f, and Br 3d elements; (G) XPS spectrum of the samples with NaBr for Na 1s element.

NaBr are matched well with the (100) and (200) planes of the standard cubic perovskite structure (ICSD 29073), demonstrating that the introduction of Na did not change the crystal structure of $CsPbBr_3$ NPLs and the Na^+ ions did not occupy any place in the lattice.[36] Besides, the diffraction peak intensity was enhanced by adding NaBr, which is a clear evidence of the optimization of grain crystallinity.[37] In addition, the XRD peak at approximately 21.4°, corresponding to the (110) plane of $CsPbBr_3$ NPLs, has nearly disappeared. This phenomenon is attributed to preferential growth along the (110) direction during the initial stage of crystal formation, which is consistent with findings reported in the literature.[38,39] X-ray photoelectron spectroscopy (XPS) was then conducted to investigate the chemical environments of the pristine and $CsPbBr_3$ NPLs with NaBr (Figure 2C). The characteristic peaks of Cs 3d, Pb 4f, and Br 3d with NaBr shifted to higher binding energies compared to those of the samples without NaBr, suggesting a more stable crystal structure (enlarged version in Figures 2D, 2E, and 2F).[40] Moreover, the ratio of Br/Pb increased from 2.61 for samples without NaBr to 2.65 for those with NaBr, indicating that Br species in NaBr are incorporated on the NPL surface to reduce the defect sites. In addition, the high-resolution XPS spectrum shows an obvious signal of Na^+ ion in the $CsPbBr_3$ NPLs with NaBr, indicating that Na^+ ions are present on the surface of the $CsPbBr_3$ NPLs (Figure 2G). As can be observed from the ^{23}Na nuclear magnetic resonance (NMR) spectra of NaBr and NaBr-$PbBr_2$ in a deuterated DMSO solution (Figure S4), the signal of Na^+ from NaBr shifts to the high field after incorporation of $PbBr_2$. This shift clearly demonstrates the interaction between Na^+ and $(PbBr_x)^{(x-2)-}$, which confirms the strong binding affinity

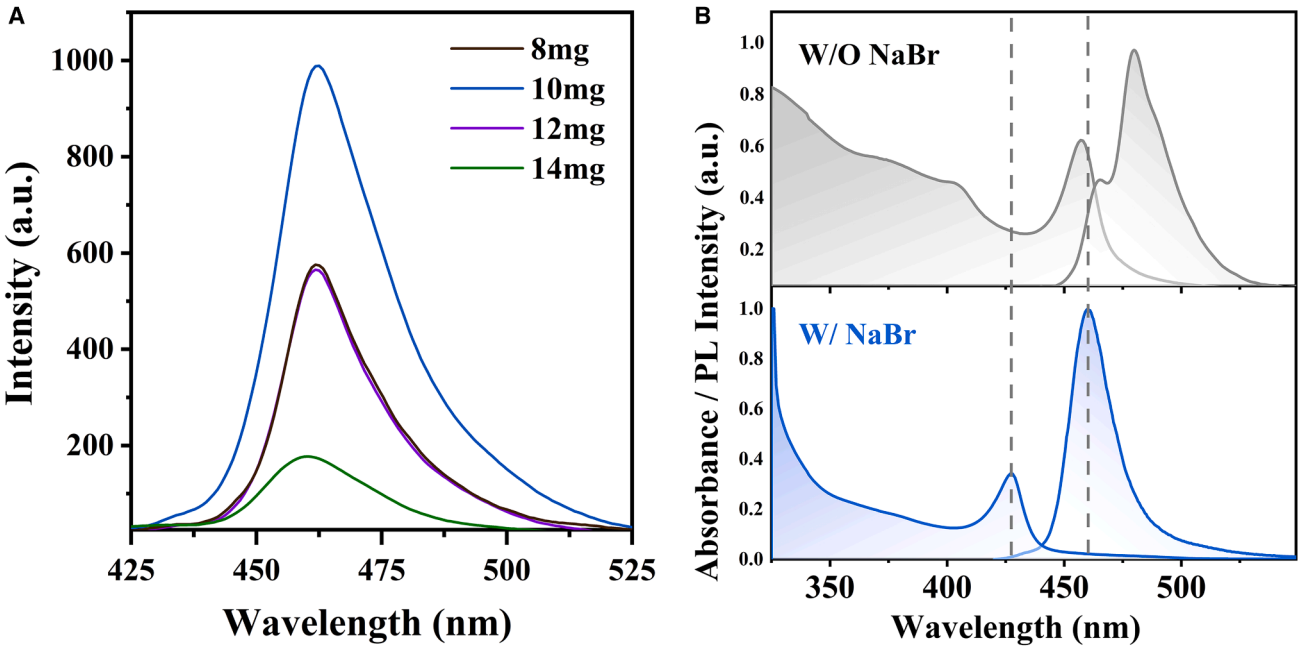

Figure 3. PL and UV-visible absorption spectra

(A) PL spectra of $CsPbBr_3$ NPLs synthesized with different masses of NaBr (8, 10, 12, and 14 mg).

(B) UV-visible absorption and PL spectra of the samples without and with NaBr.

of Na^+ ions to the NPLs. Meanwhile, the low steric hindrance of the small Na^+ ion (1.02 Å) facilitates it to cap on the surface of NPLs densely and form a ligand shell, which will limit the self-assembly between different NPLs and improve the storing stability in the solution. Based on the above results, not only does NaBr play the role of an inorganic surface ligand that caps the surface of $CsPbBr_3$ NPLs and forms an outer shell but also the Br-poor environment improves with the incorporation of NaBr.

Optical properties of $CsPbBr_3$ NPLs

To optimize the enhancement of PL with NaBr, various amounts of NaBr (8, 10, 12, and 14 mg) were added to the precursor, and the corresponding PL spectra are shown in Figure 3A. As the amount of NaBr was increased from 8 to 10 mg, the PL intensity increased. However, the PL intensity decreased with further increments in NaBr additions. The PLQY values exhibited a similar trend, with samples containing 10 mg of NaBr demonstrating the highest PLQY compared to the other samples (Figure S5), suggesting that the samples with 10 mg NaBr possess a lower surface trap density and less non-radiative recombination. The observed decrease in PL intensity and PLQY when the amount of NaBr exceeds 10 mg in the precursor can be attributed to the higher surface density of the capping ligands, which hindered the activation of the NPLs. This reduced the surface accessibility of the precursor and resulted in a lower growth rate. Consequently, the emission intensities weakened.[41] It is worth noting that the NaBr content should be carefully controlled, neither excessive nor insufficient. When the NaBr content exceeded 60 mg, an obvious redshift in the emission peak was observed (Figure S6). This can be explained by the strong interaction between NaBr and $PbBr_2$, which caused the leaching of $PbBr_2$ from the NPLs and initiated a diffusion-recrystallization process. As a result, the NPLs continued to grow and underwent phase transformation into NCs. This reduced the quantum confinement effect and caused a redshift in accordance with earlier investigations with excessive amine.[42–44] On the other hand, when the NaBr content was as low as 6 mg, despite the initial appearance of a deep blue emission in the newly synthesized sample, continuous growth of NPLs occurred after 10 h and resulted in a redshift to green emission due to the absence of quantum confinement effect (Figure S7).

We adopted $CsPbBr_3$ NPLs with 10 mg of NaBr as the modified sample for further characterization. After modification with NaBr, the absorption and emission peaks of the pristine $CsPbBr_3$ NPLs shifted from 427 to 460 nm to 457 to 480 nm, respectively (Figure 3B), which is attributed to the presence of Na shells that hinder the continuous growth of perovskites. This shift in the absorption and PL peaks is attributed to the successful synthesis of NPLs with reduced thickness, which induces deep blue luminescence through quantum confinement effects.[17,26,45] The corresponding photographs of the $CsPbBr_3$ solution are presented in Figure S8. The use of KBr is comparable to that attained with NaBr, and the $CsPbBr_3$ NPLs also exhibit emission of 460 nm (Figure S9). In general, the Urbach energy (E_U) is used to evaluate the crystal disorder; in other words, fewer defects exhibit smaller E_U.[46] From the absorbance spectra plotted on the logarithmic scale in Figure 4A, E_U was calculated by fitting the exponential part with the following equation:[47]

$$\alpha(E) = \alpha_0 \exp\left[\frac{E - E_0}{E_U}\right], \qquad \text{(Equation 1)}$$

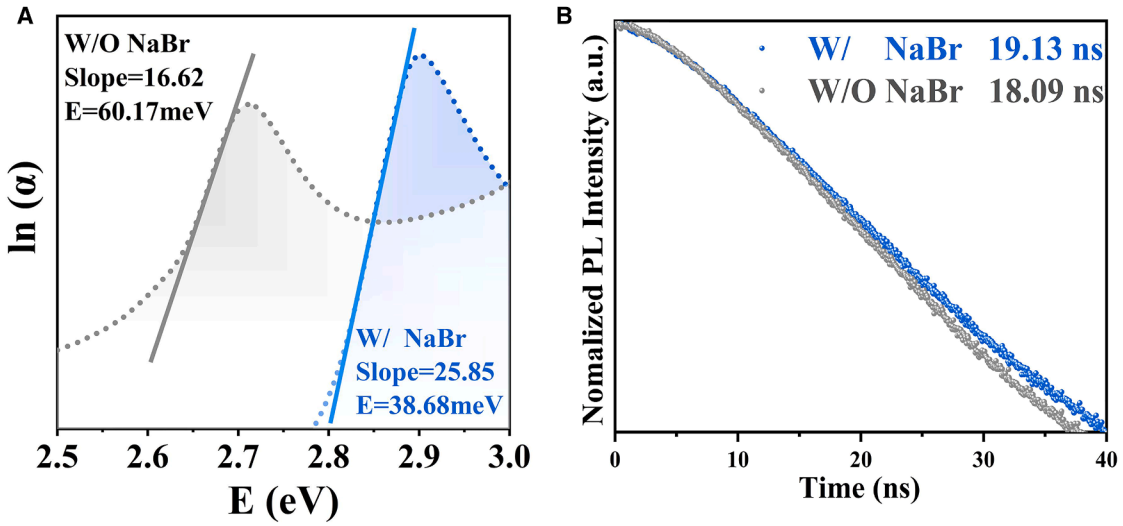

Figure 4. Optical analysis of $CsPbBr_3$ NPLs

(A) Urbach energy diagram.

(B) Time-resolved PL decay curves of $CsPbBr_3$ NPLs with and without inorganic ligand NaBr.

where α is the absorption coefficient, α_0 and E_0 are material constants, and E is the photon energy. In our case, the calculated E_U of $CsPbBr_3$ NPLs with NaBr is 38.68 MeV, which is smaller than that of the sample without NaBr (60.17 MeV), indicating that the $CsPbBr_3$ NPLs prepared with NaBr possess a very low level of defect density.[48] Time-resolved PL decay curves are shown in Figure 4B. The dependency of PL intensity on time will satisfy the single exponential form,

$$I(t) = A\exp\left(-\frac{t}{\tau}\right) + c, \qquad \text{(Equation 2)}$$

where I(t) is the observed PL intensity, A is the amplitude, and c is the constant. By fitting the two curves with single exponential function, the lifetimes of NaBr-modified (blue) and without NaBr (gray) samples were 19.13 and 18.09 ns, respectively. The larger lifetime in the sample with NaBr indicated the complete trap passivation.[49] Table S2 summarizes the optical properties of the samples both with and without NaBr, aiming to facilitate a more intuitive comprehension of the impact of NaBr.

Femtosecond (fs) transient absorption spectroscopy (TAS) was employed to further investigate the exciton dynamics. The fs-TAS of $CsPbBr_3$ samples with 0, 10, and 14 mg NaBr at 1 μJ cm^{-2} is shown in Figures 5A, 5B, and 5C. Initially, for the pristine samples without NaBr, two ground-state bleaching peaks are observed at 375 and 445 nm (Figure 5A), which correspond to the different *n* values of the complex phase distribution. Remarkably, a bleaching peak arises at 375 nm within 0.1 ps, revealing that excitons are mainly generated at low *n* value. In contrast, for $CsPbBr_3$ NPLs synthesized with 10 and 14 mg of NaBr, a single bleaching peak is clearly detected, with no impurity signals present throughout the whole delay time range (Figures 5B and 5C). These results provide evidence that the inclusion of NaBr enhances the formation of large n phases, while effectively suppressing the creation of small n phases that adversely affect exciton radiative recombination.[50] The homogeneous phase distribution enhances both energy transfer and carrier radiation recombination. Moreover, at the same delay time, the negative peak intensities of $CsPbBr_3$ NPLs with 10 mg NaBr (Figure 5B) were largely reduced compared with $CsPbBr_3$ NPLs with 14 mg NaBr (Figure 5C), agreeing well with the PL intensity quenching results. The results indicate that 10 mg NaBr-added $CsPbBr_3$ NPLs possess higher exciton radiation efficiency than the NPLs, agreeing well with the PL intensity quenching results (Figure 3).

Furthermore, the thermal stability of the NPLs was assessed by heating the NPL solution in a hot plate to 80°C (Figure 6A). The emission position exhibited negligible degradation below 3 nm, and the full width at half maximum (FWHM) increased slightly by 9 nm. The corresponding PL spectra are shown in Figure S10A. In contrast, the samples without NaBr exhibited a shift in both emission position and FWHM of up to 16 and 25 nm, respectively, showing highly unstable properties during the heating process (Figures S10B and S11). After exposure to air for 0, 48, 120, and 240 h (Figure 6B), the NPL solution exhibited minimal alterations in the emission position and FWHM. In contrast, the $CsPbBr_3$ samples without NaBr exhibited a large shift in both emission position and FWHM after 48 h (Figure S11). The sample exhibited persistent blue emission even under heating or exposure to air, indicating the ability of the Na^+ ligand shell and Br-rich environment to impede coalescence between individual NPLs and reduce the number of defect sites, thereby demonstrating colloidal stability.

To explore their application potential, a blue-LED device was fabricated using the as-prepared $CsPbBr_3$ NPLs as blue-emitting materials. Polymethyl methacrylate was added to a toluene solution of blue $CsPbBr_3$ NPLs, and then the mixture was deposited on 365-nm UV-LED chips, as shown in the diagram in the inset of Figure 7A. The electroluminescence (EL) spectra of the fabricated blue-LED is presented under bias currents of 5, 10,

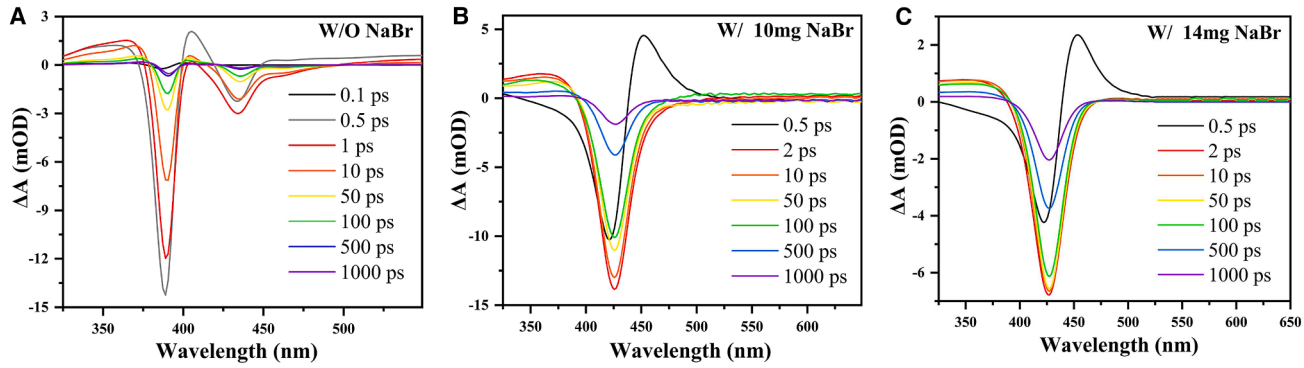

Figure 5. Fs-TA absorption spectra

(A) fs-TA absorption spectra of $CsPbBr_3$ without NaBr at different delay times.

(B) fs-TA absorption spectra of $CsPbBr_3$ with 10 mg NaBr at different delay times.

(C) fs-TA absorption spectra of $CsPbBr_3$ with 14 mg NaBr at different delay times.

15, 20, 25, 30, 40, and 50 mA (Figure 7A). The Commission Internationale de l'Eclairage (CIE) coordinates were (0.1289, 0.0887) (Figure 7B), indicating a standard blue light emission. No notable changes occurred in the spectral shape, peak position, or CIE when the driving current was increased up to 50 mA, implying good current-driven stability of the EL emission. And the EL intensity only shows a slight decrease after working for 10 h (Figure S12), which indicates a good stability of the constructed blue-LED.

In summary, highly efficient and stable inorganic ligand-capped $CsPbBr_3$ NPLs were prepared using a modified LARP method. The inorganic ligand, NaBr, and short-carbon-chain ligands can effectively regulate the crystal growth and passivate surface defects. We calculated the strong adsorption energy (Eads −2.13 eV) between Na^+ ions and the NPL surface by DFT calculation and confirmed the interaction between Na^+ and $(PbBr_x)^{(x-2)-}$ using ^{23}Na NMR. The strong binding affinity resulted in a tight Na shell on the NPL surface that achieved a quantum confinement effect. Successful synthesis of the NPLs was demonstrated using XRD, TEM, and XPS. The XPS results further confirmed that the addition of NaBr increased the stability of the crystal structure. By calculating the Urbach energy, it was found that the crystal disorder was reduced after the addition of NaBr, which further illustrates the control of NaBr in NPL growth. In summary, inorganic ligands can effectively control the synthesis of blue-emitting NPLs with potential applications in the field of blue-LEDs.

Limitations of the study

In this study, we synthesized a stable inorganic ligand-capped $CsPbBr_3$ NPL using a modified LARP method. Due to constraints imposed by our current laboratory conditions, we are temporarily

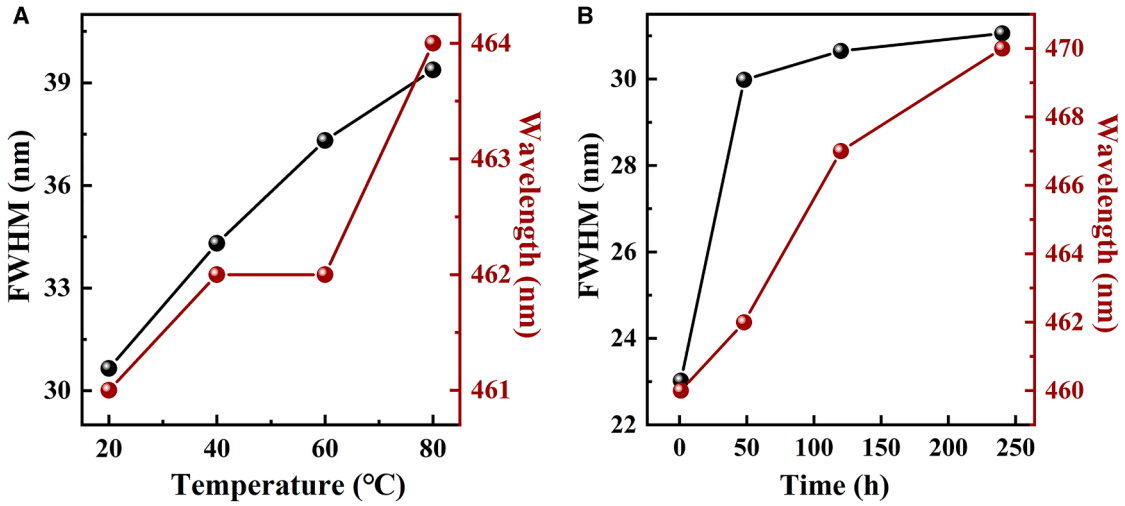

Figure 6. Stability characterization

(A) Thermal stability: FWHM and emission position after heating at different temperatures (20°C, 40°C, 60°C, and 80°C) for 15 min.

(B) Time stability: FWHM and emission position with different storage times (0, 48, 120, and 240 h) in air and room temperature.

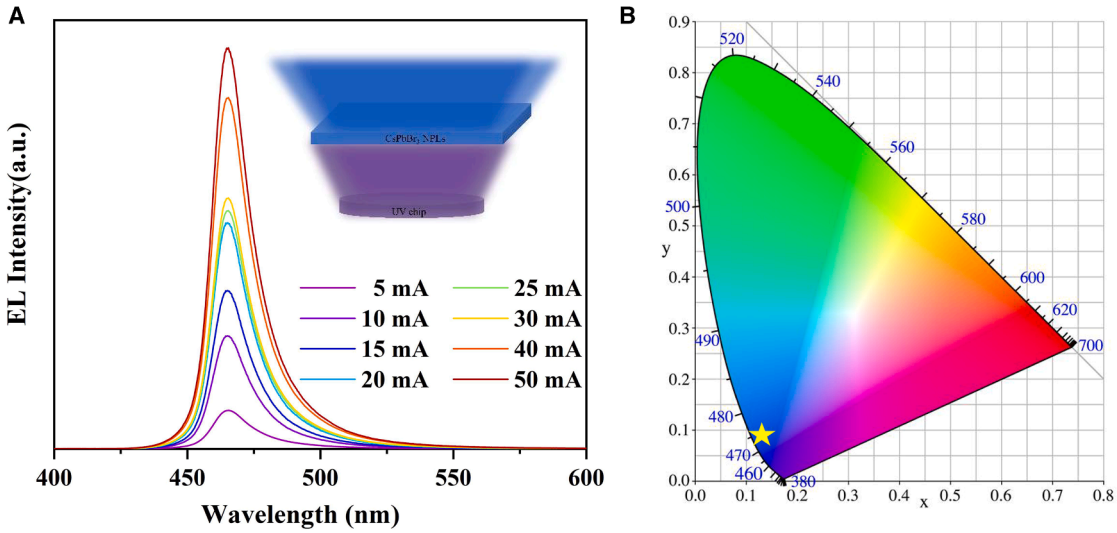

Figure 7. EL spectra and CIE chromaticity diagram of LED device

(A) Electroluminescence (EL) spectra of the blue-LED device obtained using forward currents of 5, 10, 15, 20, 25, 30, 40, and 50 mA (the inset shows a diagram of the blue-LED device).

(B) CIE chromaticity diagram of the blue-LED device under bias current of 50 mA.

unable to measure specific efficiency parameters associated with these LED devices. We remain committed to optimizing experimental conditions and strive to deliver more comprehensive and accurate data in future studies.

RESOURCE AVAILABILITY

Lead contact

Requests for further information and resources should be directed to and will be fulfilled by the lead contact, Sung Heum Park (spark@pknu.ac.kr).

Materials availability

The study did not generate new unique materials. The readers can buy the chemicals to remake the materials as mentioned in the text.

Data and code availability

- All data reported in this paper will be shared by the lead contact upon reasonable request.
- This paper does not report original code.
- Any additional information required to reanalyze the data reported in this paper is available from the lead contact upon request.

ACKNOWLEDGMENTS

This research was funded by the Nano Material Technology Development Program through the National Research Foundation of Korea (NRF), funded by the Ministry of Science and ICT (grant number 2021M3H4A1A02057007) and the BrainLink program (2022H1D3A3A01077343). This research was supported by the Foundation of Guilin University of Technology (RD2300137411) and the Qingmiao Foundation of Guangxi Zhuang Autonomous Region (DT2400003993).

AUTHOR CONTRIBUTIONS

Conceptualization, A.Z. and X.S.; methodology, A.Z.; investigation, A.Z., Z.Y., J.S., Z.W., Y.L., F.L., E.Y., and D.K.; writing – original draft, A.Z.; writing – review & editing, X.S. and S.H.P.; funding acquisition, S.H.P. and A.Z.; resources, C.S., B.R.L., and S.H.P.; supervision, S.H.P.

DECLARATION OF INTERESTS

The authors declare no competing interests.

STAR★METHODS

Detailed methods are provided in the online version of this paper and include the following:

- KEY RESOURCES TABLE
- EXPERIMENTAL MODEL AND STUDY PARTICIPANT DETAILS
- METHOD DETAILS
  - Synthesis of $CsPbBr_3$ nanoplateletes
  - Characterization techniques
  - LED fabrication
  - First principles calculations
- QUANTIFICATION AND STATISTICAL ANALYSIS

SUPPLEMENTAL INFORMATION

Supplemental information can be found online at https://doi.org/10.1016/j.isci.2025.114078.

Received: June 24, 2025
Revised: October 17, 2025
Accepted: November 13, 2025
Published: November 17, 2025

REFERENCES

1. Yang, S., Duan, Y., Liu, Z., and Liu, S.F. (2023). Recent advances in $CsPbX_3$ perovskite solar cells: focus on crystallization characteristics and controlling strategies. Adv. Energy Mater. *13*, 2201733.
2. Li, C., Belkin, D., Li, Y., Yan, P., Hu, M., Ge, N., Jiang, H., Montgomery, E., Lin, P., Wang, Z., et al. (2018). Efficient and self-adaptive in-situ learning in multilayer memristor neural networks. Nat. Commun. *9*, 2385.
3. Seth, S., Ahmed, T., De, A., and Samanta, A. (2019). Tackling the defects, stability, and photoluminescence of $CsPbX_3$ perovskite nanocrystals. ACS Energy Lett. *4*, 1610–1618.

4. Wang, Q., Wang, X., Yang, Z., Zhou, N., Deng, Y., Zhao, J., Xiao, X., Rudd, P., Moran, A., Yan, Y., and Huang, J. (2019). Efficient sky-blue perovskite light-emitting diodes via photoluminescence enhancement. Nat. Commun. *10*, 5633.

5. He, H., Mei, S., Wen, Z., Yang, D., Yang, B., Zhang, W., Xie, F., Xing, G., and Guo, R. (2022). Recent advances in blue perovskite quantum dots for light-emitting diodes. Small *18*, 2103527.

6. Zhang, S., Liu, H., Li, X., and Wang, S. (2020). Enhancing quantum yield of $CsPb(BrxCl_{1-x})_3$ nanocrystals through lanthanum doping for efficient blue light-emitting diodes. Nano Energy *77*, 105302. https://doi.org/10.1016/j.nanoen.2020.105302.

7. Naresh, V., and Lee, N. (2020). Zn(II)-Doped Cesium Lead Halide Perovskite Nanocrystals with High Quantum Yield and Wide Color Tunability for Color-Conversion Light-Emitting Displays. ACS Appl. Nano Mater. *3*, 7621–7632. https://doi.org/10.1021/acsanm.0c01254.

8. Lin, H., Wei, Q., Ng, K.W., Dong, J.-Y., Li, J.-L., Liu, W.-W., Yan, S.-S., Chen, S., Xing, G.-C., Tang, X.-S., et al. (2021). Stable and Efficient Blue-Emitting $CsPbBr_3$ Nanoplatelets with Potassium Bromide Surface Passivation. Small *17*, 2101359. https://doi.org/10.1002/smll.202101359.

9. Knight, A.J., and Herz, L.M. (2020). Preventing phase segregation in mixed-halide perovskites: a perspective. Energy Environ. Sci. *13*, 2024–2046. https://doi.org/10.1039/d0ee00788a.

10. Kong, L., Sun, Y., Zhao, B., Ji, K., Feng, J., Dong, J., Wang, Y., Liu, Z., Maqbool, S., Li, Y., et al. (2024). Fabrication of red-emitting perovskite LEDs by stabilizing their octahedral structure. NATURE *631*, 73–79. https://doi.org/10.1038/s41586-024-07531-9.

11. Yang, W., Ban, X.-X., He, X.-L., Huang, X.-M., Wang, X.-Y., Zhang, Y., and Gao, C.-H. (2024). High-Performance Green Quasi-2D Perovskite Light-Emitting Diodes via Passivated Defects. Adv. Opt. Mater. *12*, 2302664. https://doi.org/10.1002/adom.202302664.

12. Bi, C., Yao, Z., Sun, X., Wei, X., Wang, J., and Tian, J. (2021). Perovskite Quantum Dots with Ultralow Trap Density by Acid Etching-Driven Ligand Exchange for High Luminance and Stable Pure-Blue Light-Emitting Diodes. Adv. Mater. *33*, 2006722. https://doi.org/10.1002/adma.202006722.

13. Choi, I.Y., Baek, S.-D., Takaloo, A.V., Lee, S.Y., Hajibabaei, A., Kim, K.S., and Myoung, J.-M. (2022). Highly Efficient Pure-Blue Perovskite Light-Emitting Diode Leveraging $CsPbBrxCl_{3-x}/Cs_4PbBr_xCl_{6-x}$ Nanocomposite Emissive Layer with Shallow Valence Band. Adv. Opt. Mater. *10*, 2102502. https://doi.org/10.1002/adom.202102502.

14. Gao, L., Cheng, T., Gou, L., Zhang, Y., Liu, Y., Yuan, L., Zhang, X., Wang, Y., Meng, F., and Zhang, J. (2023). Eliminating Nanocrystal Surface Light Loss and Ion Migration to Achieve Bright Mixed-Halide Blue Perovskite LEDs. ACS Appl. Mater. Interfaces *15*, 18125–18133. https://doi.org/10.1021/acsami.3c02437.

15. Baek, S.-D., Wang, C., Khang, D.-Y., and Myoung, J.-M. (2023). Mixed halide perovskite nanocrystals with surface engineering based on pseudo-halide passivation and Short-Chain ligand exchange for High-Performance blue Light-Emitting diodes. Chemical Engineering Journal *455*, 140594. https://doi.org/10.1016/j.cej.2022.140594.

16. Shi, W., Zhang, X., Xie, C., Chen, H.S., and Yang, P. (2024). Blue Emitting $CsPbBr_3$: High Quantum Confinement Effect and Well-Adjusted Shapes (Nanorods, Nanoplates, and Cubes) toward White Light Emitting Diodes. Adv. Opt. Mater. *12*, 2302129. https://doi.org/10.1002/adom.202302129.

17. Bohn, B.J., Tong, Y., Gramlich, M., Lai, M.L., Döblinger, M., Wang, K., Hoye, R.L.Z., Müller-Buschbaum, P., Stranks, S.D., Urban, A.S., et al. (2018). Boosting tunable blue luminescence of halide perovskite nanoplatelets through postsynthetic surface trap repair. Nano Lett. *18*, 5231–5238.

18. Wen, Z., Cui, Z., Yang, D., He, H., Qin, S., Wang, S., Mei, S., Zhang, W., and Guo, R. (2023). Crystallization control based on A-site cation strategy for blue $FAPbBr_3$ perovskite nanoplatelets with pure emission. Appl. Surf. Sci. *615*, 156355.

19. Zheng, H., Pan, W., and Shen, W. (2018). One-step synthesis of colloidal $CH_3NH_3PbBr_3$ nanoplatelets via chlorobenzene to realize nonsolvent crystallization. Nanotechnology *29*, 455601.

20. Hautzinger, M.P., Pan, D., Pigg, A.K., Fu, Y., Morrow, D.J., Leng, M., Kuo, M.-Y., Spitha, N., Lafayette, D.P., Kohler, D.D., et al. (2020). Band edge tuning of two-dimensional Ruddlesden–Popper perovskites by a cation size revealed through nanoplates. ACS Energy Lett. *5*, 1430–1437.

21. Dong, Y., Wang, Y.-K., Yuan, F., Johnston, A., Liu, Y., Ma, D., Choi, M.-J., Chen, B., Chekini, M., Baek, S.-W., et al. (2020). Bipolar-shell resurfacing for blue LEDs based on strongly confined perovskite quantum dots. Nat. Nanotechnol. *15*, 668–674. https://doi.org/10.1038/s41565-020-0714-5.

22. Fiuza-Maneiro, N., Sun, K., López-Fernández, I., Gómez-Graña, S., Müller-Buschbaum, P., and Polavarapu, L. (2023). Ligand Chemistry of Inorganic Lead Halide Perovskite Nanocrystals. ACS Energy Lett. *8*, 1152–1191. https://doi.org/10.1021/acsenergylett.2c02363.

23. Otero-Martinez, C., Ye, J., Sung, J., Pastoriza-Santos, I., Perez-Juste, J., Xia, Z., Rao, A., Hoye, R.L.Z., and Polavarapu, L. (2022). Colloidal Metal-Halide Perovskite Nanoplatelets: Thickness-Controlled Synthesis, Properties, and Application in Light-Emitting Diodes. Advanced Materials *34*, 2107105. https://doi.org/10.1002/adma.202107105.

24. Liu, Y., Li, Y., Hu, X., Wei, C., Xu, B., Leng, J., Miao, H., Zeng, H., and Li, X. (2023). Ligands for $CsPbBr_3$ perovskite quantum dots: The stronger the better? Chem. Eng. J. *453*, 139904.

25. Jiang, Y., Sun, C., Xu, J., Li, S., Cui, M., Fu, X., Liu, Y., Liu, Y., Wan, H., Wei, K., et al. (2022). Synthesis-on-substrate of quantum dot solids. NATURE *612*, 679–684. https://doi.org/10.1038/s41586-022-05486-3.

26. Sen, A., Dutta, A., Bose, A.L., and Sen, P. (2025). Oleylammonium fluoride passivated blue-emitting 2D $CsPbBr_3$ nanoplates with near-unity photoluminescence quantum yield: safeguarding against threats from external perturbations. Chem. Sci. *16*, 735–752.

27. Lin, H., Wei, Q., Ng, K.W., Dong, J.Y., Li, J.L., Liu, W.W., Yan, S.S., Chen, S., Xing, G.C., Tang, X.S., et al. (2021). Stable and efficient blue-emitting CsPbBr3 nanoplatelets with potassium bromide surface passivation. Small *17*, 2101359.

28. Zhang, X., Zhou, Y., Peng, L., Lin, Z., Chang, Y., Zhou, Z., and Li, Y. (2022). Stable blue-emitting $CsPbBr_3$ nanoplatelets for lighting and display applications. ACS Appl. Nano Mater. *5*, 17012–17021.

29. Wen, Z., Cui, Z., He, H., Yang, D., Mei, S., Yang, B., Xiong, Z., Song, S., Bao, R., Zhang, W., et al. (2022). Exploring novel ligands with strong electron delocalization for high-performance blue $CsPbBr_3$ perovskite nanoplatelets. J. Mater. Chem. C Mater. *10*, 9834–9840.

30. Wang, H., Ye, F., Sun, J., Wang, Z., Zhang, C., Qian, J., Zhang, X., Choy, W.C.H., Sun, X.W., Wang, K., and Zhao, W. (2022). Efficient $CsPbBr_3$ nanoplatelet-based blue light-emitting diodes enabled by engineered surface ligands. ACS Energy Lett. *7*, 1137–1145.

31. Ye, F., Zhang, H., Li, W., Yan, Y., Cai, J., Gurney, R.S., Pearson, A.J., Liu, D., and Wang, T. (2019). Ligand-Exchange of Low-Temperature Synthesized $CsPbBr_3$ Perovskite toward High-Efficiency Light-Emitting Diodes. Small Methods *3*, 1800489.

32. He, H., Xing, Y., Cui, Z., Qin, S., Wen, Z., Yang, D., Xie, H., Mei, S., Zhang, W., and Guo, R. (2024). Regulating Phase Distribution of Dion–Jacobson Perovskite Colloidal Multiple Quantum Wells Toward Highly Stable Deep-Blue Emission. Small *20*, 2305191.

33. Li, H., Lu, W., Zhao, G., Song, B., Dong, W., and Han, G. (2023). Evolution and Mechanism of Cesium Lead Bromide Nanostructures in Oleylamine-Rich System by Hot-Injection Method. Adv. Mater. Interfaces *10*, 2201916. https://doi.org/10.1002/admi.202201916.

34. Huang, H., Li, Y., Tong, Y., Yao, E.P., Feil, M.W., Richter, A.F., Döblinger, M., Rogach, A.L., Feldmann, J., and Polavarapu, L. (2019). Spontaneous Crystallization of Perovskite Nanocrystals in Nonpolar Organic Solvents: A Versatile Approach for their Shape-Controlled Synthesis. Angew. Chem. Int. Ed. Engl. *58*, 16558–16562.

35. Chen, K., Zhong, Q., Chen, W., Sang, B., Wang, Y., Yang, T., Liu, Y., Zhang, Y., and Zhang, H. (2019). Short-Chain Ligand-Passivated Stable α-$CsPbI_3$ Quantum Dot for All-Inorganic Perovskite Solar Cells. Adv. Funct. Mater. *29*, 1900991. https://doi.org/10.1002/adfm.201900991.

36. Zhang, M., Zheng, Z., Fu, Q., Chen, Z., He, J., Zhang, S., Yan, L., Hu, Y., and Luo, W. (2017). Growth and characterization of all-inorganic lead halide perovskite semiconductor $CsPbBr_3$ single crystals. CrystEngComm *19*, 6797–6803. https://doi.org/10.1039/c7ce01709j.

37. Duan, J., Zhao, Y., Yang, X., Wang, Y., He, B., and Tang, Q. (2018). Lanthanide Ions Doped $CsPbBr_3$ Halides for HTM-Free 10.14%-Efficiency Inorganic Perovskite Solar Cell with an Ultrahigh Open-Circuit Voltage of 1.594 V. Adv. Energy Mater. *8*, 1802346. https://doi.org/10.1002/aenm.201802346.

38. Shi, W., Zhang, X., Xie, C., Chen, H.S., and Yang, P. (2024). Blue emitting $CsPbBr_3$: high quantum confinement effect and well-adjusted shapes (nanorods, nanoplates, and cubes) toward white light emitting diodes. Adv. Opt. Mater. *12*, 2302129.

39. Bai, H., Huang, Z., Xu, Y., Wang, Y., and Zhang, L. (2024). $CsPbBr_3$ Nanoplatelets via a Room-Temperature Postsynthetic Surface-Mediated Strategy for Blue Light-Emitting Diodes. ACS Appl. Nano Mater. *7*, 24028–24036.

40. Wang, H., Zhao, S., Liu, Y., Yao, R., Wang, X., Cao, Y., Ma, D., Zou, M., Cao, A., Feng, X., and Wang, B. (2019). Membrane adsorbers with ultrahigh metal-organic framework loading for high flux separations. Nat. Commun. *10*, 4204. https://doi.org/10.1038/s41467-019-12114-8.

41. Huang, H., Raith, J., Kershaw, S.V., Kalytchuk, S., Tomanec, O., Jing, L., Susha, A.S., Zboril, R., and Rogach, A.L. (2017). Growth mechanism of strongly emitting $CH_3NH_3PbBr_3$ perovskite nanocrystals with a tunable bandgap. Nat. Commun. *8*, 996. https://doi.org/10.1038/s41467-017-00929-2.

42. Zhao, C., He, Z., Wangyang, P., Tan, J., Shi, C., Pan, A., He, L., and Liu, Y. (2022). Bidentate Ligand-Induced Oriented Transformation of $CsPbBr_3$ Perovskite Nanocrystals into Nanowires for X-ray Photodetectors. ACS Appl. Nano Mater. *5*, 13737–13744. https://doi.org/10.1021/acsanm.2c00642.

43. Palazon, F., Almeida, G., Akkerman, Q.A., De Trizio, L., Dang, Z., Prato, M., and Manna, L. (2017). Changing the Dimensionality of Cesium Lead Bromide Nanocrystals by Reversible Postsynthesis Transformations with Amines. Chem. Mater. *29*, 4167–4171. https://doi.org/10.1021/acs.chemmater.7b00895.

44. Udayabhaskararao, T., Houben, L., Cohen, H., Menahem, M., Pinkas, I., Avram, L., Wolf, T., Teitelboim, A., Leskes, M., Yaffe, O., et al. (2018). A Mechanistic Study of Phase Transformation in Perovskite Nanocrystals Driven by Ligand Passivation. Chem. Mater. *30*, 84–93. https://doi.org/10.1021/acs.chemmater.7b02425.

45. Sen, A., and Sen, P. (2025). UV Mediated Thickness Control of Colloidal Blue-Emitting 2D $CsPbBr_3$ Nanoplatelets. ACS Appl. Nano Mater. *8*, 13975–13980.

46. Wu, Y., Wei, C., Li, X., Li, Y., Qiu, S., Shen, W., Cai, B., Sun, Z., Yang, D., Deng, Z., and Zeng, H. (2018). In Situ Passivation of $PbBr_6^{4-}$ Octahedra toward Blue Luminescent $CsPbBr_3$ Nanoplatelets with Near 100% Absolute Quantum Yield. ACS Energy Lett. *3*, 2030–2037. https://doi.org/10.1021/acsenergylett.8b01025.

47. Wright, A.D., Milot, R.L., Eperon, G.E., Snaith, H.J., Johnston, M.B., and Herz, L.M. (2017). Band-Tail Recombination in Hybrid Lead Iodide Perovskite. Adv. Funct. Mater. *27*, 1700860. https://doi.org/10.1002/adfm.201700860.

48. Ng, A., Ren, Z., Shen, Q., Cheung, S.H., Gokkaya, H.C., So, S.K., Djurišić, A.B., Wan, Y., Wu, X., and Surya, C. (2016). Crystal Engineering for Low Defect Density and High Efficiency Hybrid Chemical Vapor Deposition Grown Perovskite Solar Cells. ACS Appl. Mater. Interfaces *8*, 32805–32814. https://doi.org/10.1021/acsami.6b07513.

49. Mazzucato, S., Boonpeng, P., Carrère, H., Lagarde, D., Arnoult, A., Lacoste, G., Zhang, T., Balocchi, A., Amand, T., Marie, X., and Fontaine, C. (2013). Reduction of defect density by rapid thermal annealing in GaAsBi studied by time-resolved photoluminescence. Semicond. Sci. Technol. *28*, 022001. https://doi.org/10.1088/0268-1242/28/2/022001.

50. Wang, Y.-K., Ma, D., Yuan, F., Singh, K., Pina, J.M., Johnston, A., Dong, Y., Zhou, C., Chen, B., Sun, B., et al. (2020). Chelating-agent-assisted control of $CsPbBr_3$ quantum well growth enables stable blue perovskite emitters. Nat. Commun. *11*, 3674. https://doi.org/10.1038/s41467-020-17482-0.

STAR★METHODS

KEY RESOURCES TABLE

REAGENT or RESOURCE	SOURCE	IDENTIFIER
N,N-dimethylformamide	Sigma-Aldrich	CAS: 68-12-2
CsBr	Sigma-Aldrich	CAS: 7787-69-1
NaBr	Sigma-Aldrich	CAS: 7647-15-6
$PbBr_2$	Sigma-Aldrich	CAS: 10031-22-8
n-butylamine	Sigma-Aldrich	CAS: 109-73-9
n-octylamine	Sigma-Aldrich	CAS: 111-86-4
Methyl acetate	Sigma-Aldrich	CAS: 79-20-9
myristic acid	Sigma-Aldrich	CAS: 544-63-8
n-Hexane	Sigma-Aldrich	CAS: 110-54-3
toluene	Sigma-Aldrich	CAS: 108-88-3
Poly(methyl methacrylate) (PMMA)	Sigma-Aldrich	CAS: 9011-14-7

EXPERIMENTAL MODEL AND STUDY PARTICIPANT DETAILS

There are no experimental models (animals, human subjects, plants, microbe strains, cell lines, primary cell cultures) used in the study.

METHOD DETAILS

Synthesis of $CsPbBr_3$ nanoplateletes

$CsPbBr_3$ NPLs were synthesized using a modified LARP method. CsBr (11.9 mg), NaBr (0, 6, 8, 10, 12, 14, 40, 60, 80 mg) and $PbBr_2$ (293.6 mg) were dissolved in DMF (8 ml) to form a clear transparent precursor solution. 1 ml of precursor solution was injected swiftly into 10 ml of toluene containing 60 mg myristic acid and 60 ul n-butylamine at room temperature with vigorous stirring for 8 min. After completion of the reaction, adding 11 ml of methyl acetate and 30 ul n-octylamine into the crude solution and centrifuging at 8000 rpm (relative centrifugal force 6797 g) for 3 min, the precipitates were collected and dispersed in toluene. The toluene solution was centrifuged at 6000 rpm (relative centrifugal force 3824 g) for 1 min, the supernatant was collected and filtered.

Characterization techniques

The X-ray diffraction (XRD) patterns were obtained by PANalytical (X'Pert3-Powder) X-Ray Diffractometer. The photoluminescence and absorption spectra were detected on a Horiba (Fluorolog-QM) Photo/Fluorescence luminescence spectrometer system and JASCO (V-670) UV-Vis/NIR Spectrometer, respectively. Transmission electron microscopy (TEM) was carried out on a JEOL (JEM-F200) Field Emission Transmission Electron Microscope with a Cu grid. X-ray photoelectron spectroscopy (XPS) spectra were performed using KRATOS Analytical Ltd. (AXIS SUPRA) X-ray Photoelectron Spectrometer [Angle Resolved]. The femtosecond transient absorption spectroscopy (TAS) were obtained by sapphire laser system from Coherent (800 nm, 35 fs, 6 mJ/pulse, and 1 kHz repetition rate);TOPAS Optical Parametric Amplifier (OPA).

LED fabrication

Unpackging UV LED chip (SP3-S6PD-1) with the peak emission wavelength centered at 365 nm and electrical power of 200–300 mW was used for the fabrication of LED, which is purchased form Skybright Inc. 100 μL of $CsPbBr_3$ toluene solution (1 mL, 0.5 mg/mL) was added to 100 μL of a 20% PMMA-toluene solution. The mixed solution was agitated for 5 minutes. The mixture was treated by the ultrasonic wave for 30 min and shaken for 10 min. Then, the mixture was coated onto the UV LED chip. Finally, this chip was dried under vacuum for 1 h.

First principles calculations

We have employed the Vienna Ab Initio Package (VASP) to perform all spin-density functional theory (DFT) calculations within the generalized gradient approximation (GGA) using the Perdew-Burke-Ernzerhof (PBE) formulation. We have chosen the projected augmented wave (PAW) potentials to describe the ionic cores and take valence electrons into account using a plane wave basis

set with a kinetic energy cutoff of 450 eV. The perovskite $CsPbBr_3$ NPLs were modeled with 2 × 1 supercells, and the (100) surface was investigated in this work. Partial occupancies of the Kohn−Sham orbitals were allowed using the Gaussian smearing method and a width of 0.05 eV. The electronic energy was considered self-consistent when the energy change was smaller than 10^{-5} eV. A geometry optimization was considered convergent when the energy change was smaller than 0.02 eV $Å^{-1}$. A 6×6×2 k-point grid in the Brillouin zone was used for k-point sampling.

QUANTIFICATION AND STATISTICAL ANALYSIS

No methods were used to determine whether the data met the assumptions of the statistical approach.